Journal of Medical and Biological Engineering (2020) 40:71–81
https://doi.org/10.1007/s40846-019-00481-y

ORIGINAL ARTICLE

3D Bioprinted Integrated Osteochondral Scaffold-Mediated Repair of Articular Cartilage Defects in the Rabbit Knee

Yadong Yang[1] · Geng Yang[1] · Yongfei Song[1] · Yimeng Xu[1] · Siyu Zhao[1] · Wenyuan Zhang[1]

Received: 12 February 2019 / Accepted: 18 June 2019 / Published online: 9 July 2019

Abstract

Objective To demonstrate that a 3D-bioprinted integrated osteochondral scaffold can provide improved repair of articular cartilage defects in the rabbit knee compared to that reported for traditional tissue-engineering methods.

Results Bone marrow mesenchymal stem cells were differentiated into osteoblasts and chondrocytes as seed cells and mixed with the corresponding bone and cartilage scaffold materials. An integrated osteochondral biphasic scaffold was fabricated via 3D-bioprinting technology through successive natural overlays of the printed material and used to repair full-thickness articular cartilage defects in the rabbit knee. Histological and biomechanical assessment of repaired tissue at 6 months post-transplantation showed almost complete repair of injured articular surfaces and presence of hyaline cartilage. A boundary existed between the transition and repair zones. The Wakitani histological score was 5.50 ± 2.07 points; maximum load was 183.11 ± 35.20 N. Repaired cartilage was integrated firmly with the subchondral bone and almost assimilated with surrounding cartilage and bone tissues.

Conclusion The 3D bioprinted integrated osteochondral scaffold achieved double bionic effects on the scaffold composition and structure, and it is expected to offer a new strategy for articular cartilage repair and regeneration.

Keywords Sodium alginate · Hydroxyapatite · Bone marrow-derived mesenchymal stem cell · 3D bioprinting · Articular cartilage defect · Scaffold material

1 Introduction

Articular cartilage damage is commonly caused by trauma or inflammation; however, the injured cartilage does not naturally regenerate. If not treated, the damage often develops into degenerative arthritis and may lead to the loss of entire joint function. Moreover, articular cartilage lesions are often accompanied by subchondral lesions that impact cartilage metabolism, triggering a vicious circle that impairs cartilage repair over the long-term and causes difficulties in clinical treatment [1]. Therefore, the holistic treatment of osteochondral injury poses a considerable clinical challenge.

In traditional tissue engineering, a structural scaffold is first prepared from biological material, then seed cells, which directly mediate the repair effects, are inoculated onto the scaffold to construct a tissue-like body. This method can be used to construct osteochondral tissues, although the seed cells are readily lost and not conducive to the fabrication and growth of engineered tissues with complex structures and functions. In addition, a weakly connected cartilage–cartilage interface alone is insufficient to effect repair [2, 3]. The development of tissue engineering provides new approaches for osteochondral regeneration and repair, especially for large-area osteochondral defects [4, 5]. The simple cartilage repair has been replaced by the overall repair of cartilage and subchondral bone [6, 7]. Three-dimensional (3D) printing is a highly attractive technological approach for the layer-by-layer fabrication of complex structures. Tissue and organ structures can be prepared by printing materials and cells simultaneously through 3D printing technology [8].

Consequently, a layered structure of cartilage and subchondral bone is essential for a cartilage repair scaffold material to provide mechanical support of the subchondral bone and promote scaffold anchoring to the host tissue [9]. The subchondral bone supports cartilage regeneration and integration, anchorage with the host tissue, and provides a

✉ Wenyuan Zhang
zhangwy61@zjams.com.cn

[1] Institute of Bioengineering, Zhejiang Academy of Medical Sciences, 182 Tian Mu Shan Road, Hangzhou 310013, Zhejiang Province, China

favorable mechanical environment in the weight-bearing joint to enhance cartilage tissue regeneration performance [10]. Constructing integrated tissue-engineered osteochondral composite scaffolds is expected to effectively address these issues [11]. For example, a diphasic integrated scaffold constructed of two different scaffold materials, with bone and cartilage scaffold layer composition and structure designed according to the needs of bone and cartilage growth, can provide better characteristics for tissue repair.

The choice of seed cells is also important. Bone marrow mesenchymal stem cells (BMSCs) are currently the most studied cells in bone and cartilage tissue engineering [12, 13]. Compared with mature chondrocytes, BMSCs exhibit better cell distribution, and cartilage and subchondral bone regeneration during cartilage damage repair in various animals [14]. BMSCs also exhibit low immunogenicity [15] and strong bone and cartilage differentiation potentials [16, 17].

According to different articular cartilage and subchondral bone composition and structure characteristics, 3D bio-printing technology was used to accurately transport, locate, and assemble living cells with the matrix materials under computer-aided design control and air pressure driving to construct an integrated osteochondral biphasic scaffold carrying seed cells with alginate/gelatin as the cartilage layer, and alginate/gelatin/hydroxyapatite gel as the bone layer. The integrated osteochondral scaffold was prepared by successive natural overlays of the printed material. Specific spatial arrangement of cells and extracellular matrix materials was achieved in this scaffold, to construct an osteochondral tissue precursor with complex 3D structure, tissue structure, and function approximating that of the body. The prepared integrated osteochondral scaffold was then implanted into the articular cartilage defect in a rabbit, and the repair effect was explored.

2 Materials and Methods

2.1 Materials

Sodium alginate (low viscosity; Sigma), hydroxyapatite (Shanghai Gold Wheat Biotechnology Co., Ltd., China), gelatin (Sigma), calcein-AM (CAM)/propidium iodide (PI) (Solarbio, Beijing, China), fluorescence inverted microscope (IX73; Olympus), 3D bioprinter (BioScaffolder 2.1, GeSiM, Germany), and mechanical tester (Shanghai QiXiang Testing Instrument Co., Ltd., China) were used. Healthy New Zealand white rabbits were provided by the Zhejiang Experimental Animal Center (license No. SCXK (Zhejiang) 2013-0055).

2.2 Printed Material Preparation and Disinfection

Prepare 10 ml of the mixed solution containing 8% sodium alginate and 5% gelatin as the cartilage-like material. As above, make 10 ml of the mixed solution containing 8% sodium alginate, 5% gelatin, and 4% hydroxyapatite as the bone layer material. Observe the transition of the mixed solution (8% sodium alginate and 5% gelatin) from sol to gel state at different temperatures and the morphology after cross-linking with 5% $CaCl_2$.

For sterilization, the two materials were placed in small beakers with the cap tightened, and heated at 70 °C, 30 min per day for 3 consecutive days. The prepared materials were stored at 4 °C before use.

2.3 Isolation, Purification, Amplification, Induction, and Differentiation of Rabbit BMSCs

Two 1-month-old New Zealand white rabbits were anesthetized using 3% sodium pentobarbital (1.1 ml/kg) via ear vein injection. Bone marrow samples were extracted from the rabbit iliac spine under aseptic conditions and BMSCs were isolated and purified by density gradient centrifugation and adherent culture. Osteogenic and chondrogenic differentiation were induced in BMSCs [18–20], as seed cells for subsequent experiments to construct corresponding tissue-engineered bone and cartilage analogs. The mineralized nodules forming after osteogenic induction were stained with Von Kossa staining, and toluidine blue staining was performed after chondrogenic induction.

3 3D Printing of the Integrated Osteochondral Scaffold

Bone (10 ml) and cartilage (10 ml) layer materials were heated and dissolved at 37 °C; osteogenic- and cartilage-induced BMSCs (2 ml) were added to the corresponding material at 3×10^7 cells/ml final cell concentration, uniformly stirred, then loaded into the printing cylinder. Printing parameters were: temperature 37 °C, air pressure 270 kPa, printed needle aperture 0.4 mm. The prepared scaffold was square shaped (8 mm side length), 6 strips per layer, 0.25 mm layer height, 28 layers in total.

The osteoid tissue part, composed of osteogenic BMSCs and the bone layer material, was continuously printed and extruded by the 3D printer under computer-aided design control and air pressure driving. After 14 layers were printed, the printer nozzle was automatically converted as reported [21]. The mixed solution (cartilage-induced BMSCs and cartilage layer material) was extruded by continuous printing

and naturally superposed on the bone analog; 14 layers were also printed to form the integrated osteochondral scaffold. Immediately after the end of printing, 5% $CaCl_2$ solution was added dropwise to complete the cross-linking curing instantaneously, achieving sol–gel scaffold transformation to ensure the feasibility and continuity of the biomaterial formation. The printed integrated scaffold was placed into 24 well culture plates, and an appropriate amount of low glucose-Dulbecco's modified Eagle medium (DMEM) complete was added and cultured at 37 °C in the 5% CO_2 incubator. The osteochondral tissue was cultured in vitro for 3 days. Cell growth in the scaffold was observed by CAM/PI fluorescence staining. Mechanical properties of scaffold such as maximum load and compressive strength were detected by mechanical tester and surface morphology was observed by scanning electron microscopy (SEM).

3.1 Cytotoxicity Test of the Simple Integrated Scaffold (Without Cells)

Leaching solutions of the printed integrated scaffold (without cells) were prepared at different times: the scaffold was placed into the centrifuge tube, 2 ml low glucose-DMEM complete added, and shaken at 100 r/min, 37 °C. At 1, 3, 5, and 7 days, the leaching solution was collected, and replaced with fresh medium.

BMSCs (1×10^5 cells/ml, 100 µl per well) were inoculated into 96 well plates and incubated at 37 °C overnight in CO_2. The medium was replaced with leaching solution obtained at different times (200 µl/well, 3 wells per sample). Low glucose-DMEM complete was added into 3 wells as a negative control. After 48 h culture, the supernatant was replaced with MTT (100 µl, 500 µg/ml), and incubated at 37 °C in the dark for 4 h. The supernatant was then replaced with 150 µl of DMSO and shaken for 10 min. The optical density (OD) value was measured at 490 nm.

3.2 Osteochondral Defects on the Trochlea of the Femur and Scaffold Transplantation

Thirty-six New Zealand white rabbits, aged 3.5 months, weighing about 2.3 kg, male or female, were anesthetized by intravenous injection of 3% sodium pentobarbital (1.1 ml/kg) into the ear vein. Surgical incisions were made aseptically inside the knee joint of both hind limbs and the patellas were slid outward to the knee joint to expose the cartilage surface of the femoral joint. An electric drill was used to cause a cylindrical defect, 4.0 mm in diameter and 7 mm in depth, on the trochlea of the femur. The defects were deep into the subchondral bone, with the appearance of blood oozing on the bone surface.

Rabbit models were randomly divided into 3 groups with 12 rabbits (24 knees) in each group. For the experimental group, the integrated osteochondral scaffold was implanted into the osteochondral defect after cultured in low glucose-Dulbecco's modified Eagle medium (DMEM) complete for 7 days. The cartilage-like part of the scaffold faced upward, with the bone-like part placed next to the subchondral bone. In the control group, the integrated scaffold (without cells) was similarly implanted into the osteochondral defect. The blank group received no intervention. After suturing of the joint cavity and skin in each group, penicillin (100,000 IU/ml) was injected into the ear vein, 4 ml per day, for 3 consecutive days. The rabbit knee joint was not fixed post operation. The animal feeding environment and the basic feed were provided by the Zhejiang Experimental Animal Center. The animal disposal during the experiment met the animal ethical standards. All the rabbits were caged individually, had no restrictions on activities, and had free access to food and water.

3.3 Postoperative Observation of Articular Cartilage Defects

Half of the animals in each group were killed at 3 and 6 months after transplantation. Half of the specimens were used for histological examination (pathological section and hematoxylin–eosin staining) and the others for mechanical testing (new bone-cartilage mechanical testing). Gross observation of the specimens was also conducted. Wakitani histological scoring [22] was used to assess and quantify the repair effect.

3.4 Statistical Analysis

Data are expressed as the mean ± SD and analyzed using SPSS13.0. Data for multiple comparisons were performed by one-way ANOVA. A value of $P < 0.05$ was considered significant.

4 Results

4.1 Printed Material Characterization

The mixed solution could change from sol (37 °C) to gel (10 °C) depending on temperature, and this transformation was reversible. After adding 5% $CaCl_2$ solution into the mixed solution, the cross-linking curing being happened instantaneously from the surface to the inside. After curing, the material shrank significantly and broke away from the bottle wall. When the material is inverted in the sol state, it would flow down in the shape of a tongue (Fig. 1).

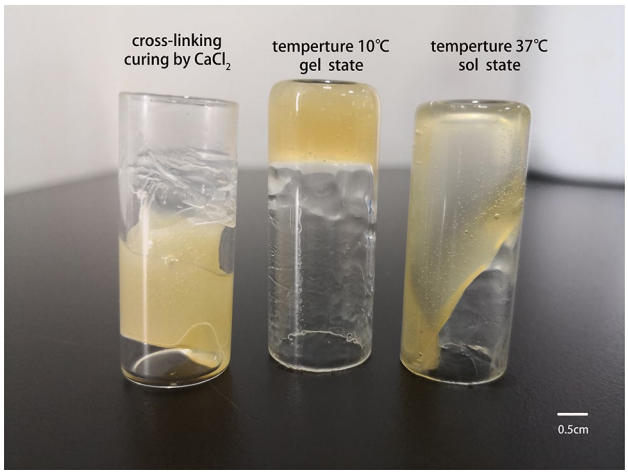

Fig. 1 The mixed solution characterization. The solution at 37 °C (right) and after gelation at 10 °C (middle). $CaCl_2$ was added for cross-linking curing (left)

4.2 Isolation, Purification, Amplification, Induction, and Differentiation of Rabbit BMSCs

A small amount of BMSCs adhered at 2 days after isolation and purification. These cells were translucent and fusiform-shaped and covered a single layer after 5 days of culture. The growth rate of cells increased obviously after passage, with a single layer covered after 3 days of culture. A small number of mineralized nodules formed after 3 weeks of osteogenic induction. Over time, mineralized nodules increased in number and formed pieces after 6 weeks of induction (Fig. 2b). No mineralized nodules were observed in the non-induced BMSCs (Fig. 2a). After 4 weeks of cartilage induction, the cytoplasm was positive for toluidine blue staining, whereas that of non-induced BMSCs was negative (Fig. 2c, d).

5 3D-Printed Integrated Osteochondral Scaffold

The integrated osteochondral scaffold had 28 layers, of which 14 were bone-like and the others were cartilage-like. These layers were continuously printed, extruded, and naturally stacked without physical separation. The printed scaffold was completely shaped with no collapse (Fig. 3a). It had pores on all sides and connected with each other. The pore size was about 0.5 mm (Fig. 3b). Cells growing in clusters adhered to the scaffold as shown by scanning electron microscopy (Fig. 3c). After 3 days of in vitro culture, CAM/PI double staining showed that stained cells were mainly around the scaffold pores, whereas the cells inside the scaffold dispersed and grew. There were stained cells per visual field (Fig. 3d–f).

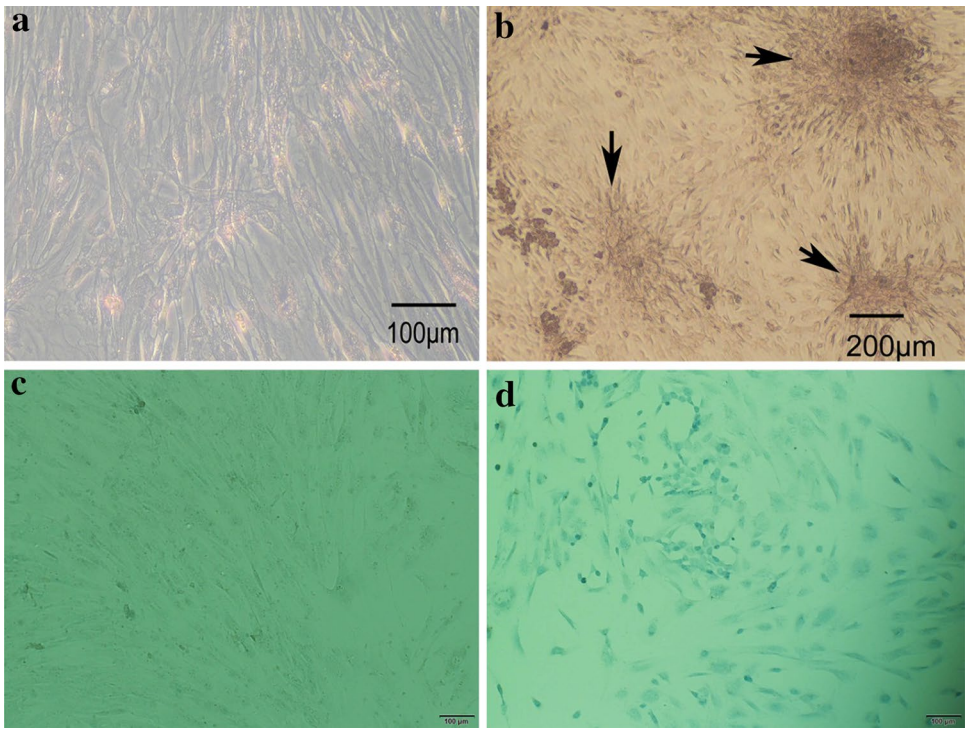

Fig. 2 Mineralized nodules in BMSCs were stained with Von Kossa staining at 6 weeks after osteogenic induction, and with toluidine blue staining at 4 weeks of chondrogenic induction (100×). Non-induced BMSCs were set as controls. **a** Non-induced BMSCs showed no formation of nodules after 6 weeks of culture and were negative for Von Kossa staining (100×). **b** Mineralized nodules (black arrows) in osteogenic-induced BMSCs (40×). **c** Non-induced BMSCs were negative for toluidine blue staining (100×). **d** Stained cytoplasm in chondrogenic-induced BMSCs (100×)

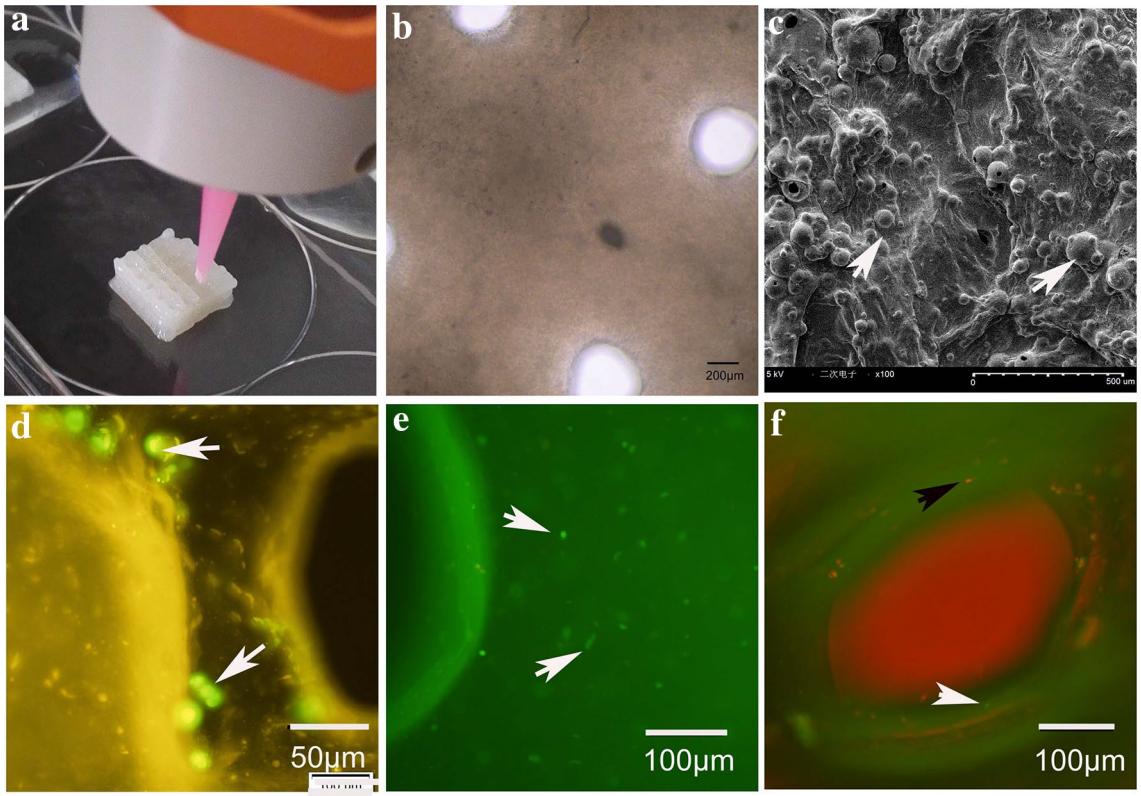

Fig. 3 Observation of integrated osteochondral scaffolds. **a** Appearance of the 3D printed scaffold. **b** Cross-sectional view of the printed 4 layer-scaffold. The pore size is about 200 μm. (40×). **c** SEM observation of the scaffold surface (cartilage-like layer) after 7 days of in vitro culture. White arrows indicate cells (100×). **d** Cells (white arrows) near a scaffold pore after 3 days of culture (200×). **e** Inconsistent fluorescence intensities of cells at different levels of the scaffold after 7 days of culture (100×). **f** CAM/PI staining for cell survival and death on the scaffold after 3 days of culture. White arrow (living cells; green dots), black arrow (dead cells; red dots) (100×)

5.1 Cytotoxicity of the Simple Integrated Scaffold (Without Cells)

Following culture in the scaffold leaching solution for 48 h, MTT assay showed that the cell survival rate was 61.7% in the 1-day scaffold leaching solution, although microscopic examination showed good cell growth. Cell viabilities for 3-, 5-, 7-day scaffold leaching solutions were all over 70% (Fig. 4).

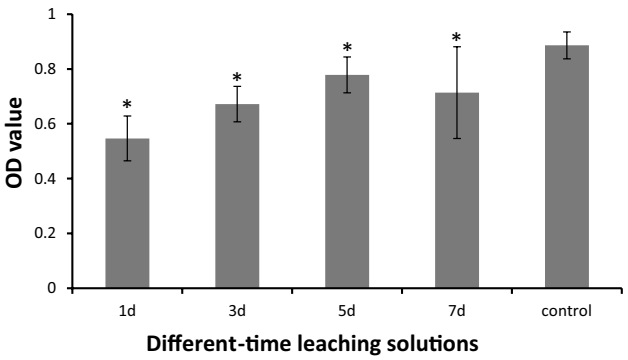

Fig. 4 Cell viability (OD value) of BMSCs in different-time leaching solutions at 48 h of culture. *P < 0.05 compared with the blank control

5.2 Repair of Articular Cartilage Defects

5.2.1 Gross Observation

In the blank group, after 3 months, the defect was unrepaired, the defect size was unchanged, the surrounding bone was damaged, and red loose tissue or yellow exudate filled the defect. After 6 months, the defect size still showed no significant change, and the defect was not repaired (Fig. 5b).

In the control group, the joint fluid was clear at 3 months after implantation of the simple scaffold, and there was no significant change in the defect size. Fibrous tissues, soft and bright red, filled the defect, the surface was free of cartilage tissue, and there was no obvious bone destruction and no new cartilage around the defect. After 6 months of scaffold implantation, the surface of the femoral trochlea had no voids but was still uneven. Fibrous-like tissues, transparent and soft, appeared as repaired tissues (Fig. 5c).

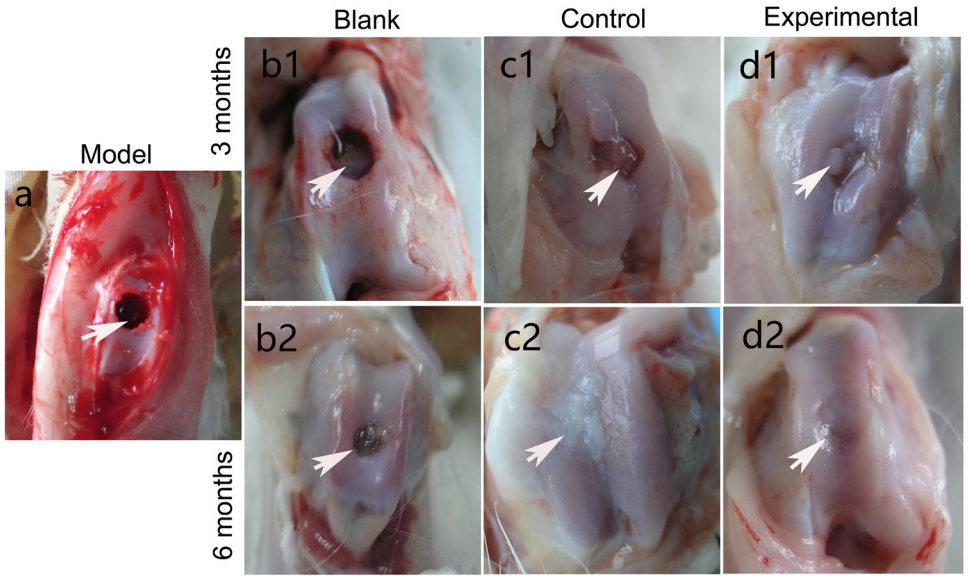

Fig. 5 Gross observation of articular cartilage defects at different times after scaffold implantation. **a** Preparation of the cartilage defect model: a cylindrical cartilage defect with a diameter of 4 mm and a depth of about 7 mm was made with electric drill prior to scaffold implantation. **b** Blank group at 3 (**b1**) and 6 (**b2**) months post-operation. **c** Simple scaffold (without cells) at 3 (**c1**) and 6 (**c2**) months after implantation. **d** Integrated osteochondral scaffold after 3 (**d1**) and 6 (**d2**) months of implantation

In the experimental group, after 3 months of scaffold implantation, the joint fluid was clear, and the defect size was significantly reduced. Moreover, hard spongy bone tissues filled the defect, and the color was bright red. Several flaky white hyaline cartilage tissues that were similar to the surrounding cartilage grew around the defect. After 6 months of scaffold implantation, the articular surface was almost repaired but was slightly lower than the surrounding cartilage. Transparent cartilage tissues were observed in the defect (Fig. 5d).

5.2.2 Histological Findings

In the blank group, the cartilage defect was unrepaired at 3 months after surgery, and only thin fibrous tissue appeared on the defect surface, with no normal articular cartilage structure and few subchondral plates and trabecular bone. At 6 months after surgery, the pathological section showed no tissue repair in the defect area, with only the granulation tissue adhering to the surrounding cartilage. No normal articular cartilage structure was apparent (Fig. 6a, b). In the control group, at 3 months after implantation of the simple scaffold (without cells), the defect area was repaired by fibrous connective tissues that were concentrated from the periphery to the central area of the defect. This area from the periphery to the center was temporarily indicated as the "transition zone," which had basic articular cartilage structure, and the central area was still not completely filled by fibrous connective tissues. At 6 months after scaffold implantation, hyaline cartilage and fibrocartilage tissue were mixed in the transition zone. The defect center was repaired by fibrocartilage tissues; however, the repaired cartilage thickness was markedly thinner than that of normal hyaline cartilage. A fissure existed at the junction of the transition zone and the normal cartilage, indicating that under the action of external force, the original tissue and the new tissue at the junction were easily separated, and there was no obvious delamination between the repaired tissue and the subchondral plate (Fig. 6c, d).

In the experimental group, at 3 months after integrated osteochondral scaffold implantation, the defect was basically repaired but the surface was uneven. The repaired cartilage tissue structure was disordered. The repaired tissues in the transition zone basically exhibited hyaline cartilage structural features, and fibrocartilage tissues mainly filled the central area of the defect. The repaired tissues in the transition zone showed weak binding to and were even separated from the thickened superficial layer of surrounding cartilage tissues at the junction. At 6 months after implantation, hyaline cartilage tissues appeared as repaired tissues, basically having articular cartilage structure. Subchondral plate and trabecular bone structure was essentially normal. The repaired central area was slightly lower than the surrounding cartilage. There was still a boundary between the transition zone and the repaired central area, and no obvious delamination occurred (Fig. 6e1, f).

5.2.3 New Bone-Cartilage Mechanical Results

At 7 days of in vitro culture, compared with the normal data of articular cartilage, the scaffold almost exhibited no pressure bearing function. The maximum load and compressive strength at 3 and 6 months after implantation of the integrated osteochondral scaffold into the cartilage defect are shown in Table 1.

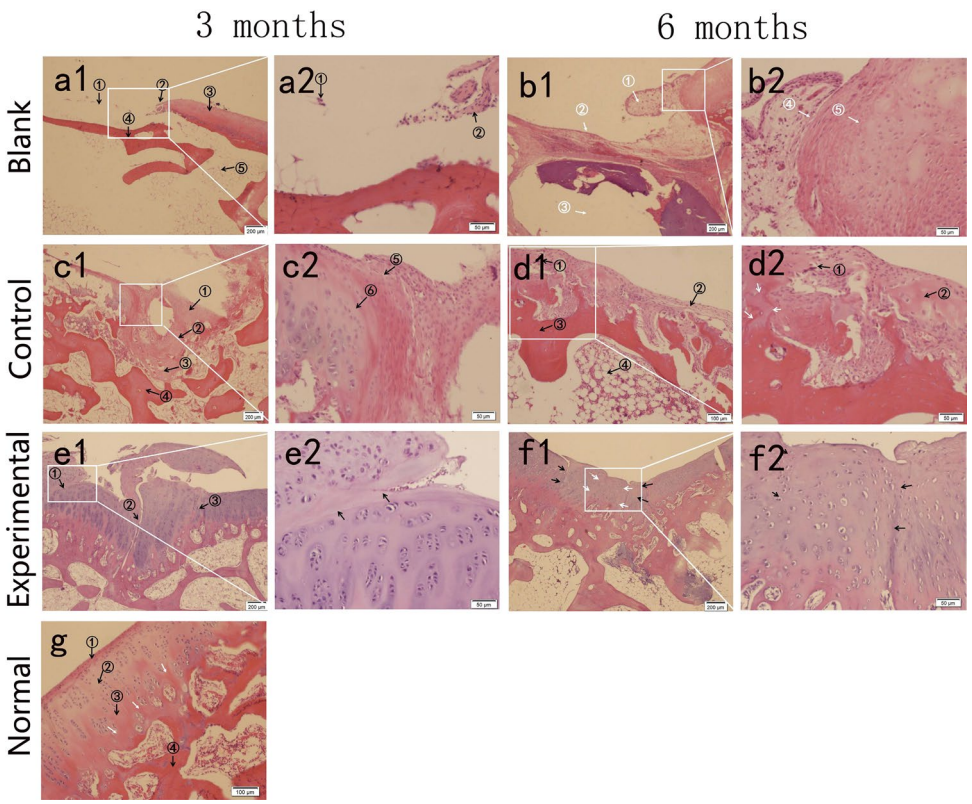

Fig. 6 Pathological observation of the injured articular cartilage using hematoxylin–eosin staining at different times after scaffold implantation (**a1**–**f1**: 40×; **a2**–**f2**: 200×; g: 100×). **a1** Blank group at 3 months post operation. Arrow 1, thin fibrous tissue; arrow 2, binding of the defect to margin; arrow 3, surrounding normal cartilage tissue; arrow 4, loose subchondral plate; arrow 5, scarce trabecular bones. **a2** Enlargement of the white frame portion of **a1**. Arrow 1, thin fibrous tissues; arrow 2, fibrous tissues growing from the edge of the defect. **b1** Blank group at 6 months post operation. Arrow 1, granulation tissues growing around the surrounding cartilage; arrow 2, granulation tissue growing on the defect inner surface; arrow 3, unrepaired defect. **b2** Enlargement of **b1**. Arrow 4, junction of the granulation tissue and the surrounding articular cartilage surface of the defect; arrow 5, boundary between the thickened superficial layer and intermediate layer of the articular cartilage. **c1** Control group at 3 months after simple scaffold (without cells) implantation. Arrow 1, superficial part of the repaired tissues in the "transition zone", mainly the fibrous connective tissues; arrow 2, intermediate layer of the repaired tissue, mainly the denser fibrocartilage; arrow 3, deep layer of the repaired tissues; arrow 4, thickened subchondral plate. **c2** Enlargement of **c1**. Arrow 5, junction of the transition zone and the articular cartilage surface around the defect; arrow 6, boundary between the superficial and intermediate layers of the thickened articular cartilage. **d1** Control group at 6 months post operation. Arrow 1, junction of the repaired tissue in the "transition zone" and the surrounding cartilage tissue. The repaired-original tissue juncture presented with interlaced growth repair. Arrow 2, thin collagen fibrous tissues, without normal hyaline cartilage structure. Arrow 3, subchondral plate. Arrow 4, trabecular bone. **d2** Enlargement of **d1**. Arrow 1, fissure between the new tissue and surrounding cartilage tissue. Arrow 2, interlaced growth of transparent cartilage-like tissues in the repaired fibrocartilage tissues in the "transition zone". **e1** Experimental group at 3 months after integrated osteochondral engineered tissue implantation. Arrow 1, boundary of the "transition zone" and the repaired central zone. Arrow 2, junction of the repaired tissue in the "transition zone" and the superficial layer of the surrounding cartilage. Arrow 3, junction of the superficial layer of the thickened cartilage and the normal cartilage. **e2** Enlargement of **e1**. Arrow, boundary between the "transition zone" and the repaired center zone. **f1** Experimental group at 6 months after engineered tissue implantation. Black arrow, juncture between the new tissue and the surrounding cartilage; white arrow, junction of the interlaced repair area and the repaired central zone. **f2** Enlargement of **f1**. Arrow, boundary between the "transition zone" and the repaired center zone. **g** Normal rabbit articular cartilage section. Arrow 1, superficial layer of articular cartilage mainly composed of collagen fibers. Arrow 2, intermediate layer of articular cartilage. Arrow 3, deep layer of articular cartilage, in which the chondrocytes were arranged in a bead shape. Arrow 4, subchondral plate. Three white arrows, tide mark

5.2.4 The Wakitani Histological Scoring for Quantification of the Repair Effect on Articular Cartilage Defects

The Wakitani histological scoring has the range of 0–14: score 0 refers to the normal cartilage, and score 14 refers to completely unrepaired tissue. After 6 months of scaffold implantation, the experimental group had a better repair of articular cartilage defects, with a total score of 5.50 ± 2.07. The Wakitani score was 9.33 ± 1.37 in the control group and 14 in the blank group (basically unrepaired). There were no significant differences between the three groups at 3 months after scaffold implantation ($P > 0.05$), whereas significant

Table 1 New bone-cartilage mechanical testing results

Index	Normal articular cartilage	Experimental			Control	
		0 month	3 months	6 months	3 months	6 months
Maximum load (N)	480.09 ± 64.63	4.64 ± 1.01[a]	33.15 ± 10.74[a]	183.11 ± 35.20[a]	27.32 ± 7.62[ab]	96.33 ± 20.58[ac]
Compressive strength (MPa)	30.34 ± 4.18	0.29 ± 0.07[a]	2.07 ± 0.64[a]	11.44 ± 2.21[a]	1.70 ± 0.75[ab]	6.04 ± 1.43[ac]

Data are expressed as the mean ± SD (n = 6 per group)

[a]$P < 0.01$, vs. the normal articular cartilage

[b]$P < 0.05$, vs. concurrent transplantation in the experimental group

[c]$P < 0.0.1$, vs. concurrent transplantation in the experimental group

differences appeared at 6 months after scaffold implantation ($P < 0.05$; Table 2).

6 Discussion

To establish a suitable matrix environment for the differential development of articular cartilage and bone tissues, 3D bio-printing technology was used to directly assemble lineage-induced BMSCs and matrix materials through accurate transportation and positioning to construct an integrated osteochondral biphasic scaffold carrying seed cells with alginate/gelatin as the cartilage layer and alginate/gelatin/hydroxyapatite gel as the bone layer. A mixed solution of osteogenic BMSCs and hydroxyapatite powder/sodium alginate/gelatin was used to print the bone layer, whereas a mixed solution of chondrogenic BMSCs and sodium alginate/gelatin was used to print the cartilage layer. Different layers of the integrated scaffold were tightly anchored and formed as a complete whole, obviating issues of incomplete integration between cartilage and subchondral bone at the natural interface. Consistent with this, pathological sections from the control and experimental groups showed that the repaired tissue and the subchondral bone were interlaced without obvious stratification and separation, indicating the formation of nearly normal articular cartilage structure.

Given the similarity in structure, composition, and mechanical properties of hydrogel and cartilage extracellular matrix, current cell or tissue printing techniques are mainly based on cell-based hydrogel 3D printing technology. The basic requirements for 3D printed hydrogel scaffolds carrying cells include: (1) the hydrogel can be rapidly formed in situ and maintain the initial form after deposition on the bench; (2) the printed scaffold maintains cell activity and function; (3) the printed scaffolds are easy to post-process; and (4) the printed scaffolds have good pore size, interpenetration, and mechanical properties. Sodium alginate and hydroxyapatite substantially meet the requirements for 3D printed materials of osteochondral scaffolds.

Sodium alginate, a polysaccharide extracted from natural brown algae, is similar to glycosaminoglycans in the extracellular matrix and has good water solubility and biocompatibility. Sodium alginate can be rapidly combined with calcium ions to form a stable gel [23] in situ with little cell damage. Its gel-like network structure provides adequate attachment surface, allowing chondrocytes to grow in a more physiologically similar environment, which helps the cells to remain active and secrete large amounts of matrices. Hydroxyapatite has favorable osteoconductivity, osteoinductivity, and biological activity [24], encouraging firm binding between the bone layer and the surrounding tissue [25]. This promotes cartilage layer fixation to firmly anchor the entire restoration in the defect at an early stage, providing

Table 2 Quantification of the repair effect on articular cartilage defects based on the Wakitani histological scores (n = 6)

Index	Experimental group		Control group		Blank group	
	3 months	6 months	3 months	6 months	3 months	6 months
Cell shape	3.33 ± 0.52	1.5 ± 0.55	3.67 ± 0.52	2.17 ± 0.41	4 ± 0	4 ± 0
Base dyeing	2.67 ± 0.52	1.17 ± 0.41	2.83 ± 0.41	1.67 ± 0.52	3 ± 0	3 ± 0
Surface regulations	2.83 ± 0.41	1.50 ± 0.55	2.83 ± 0.41	3 ± 0	3 ± 0	3 ± 0
Cartilage thickness	2 ± 0	1.00 ± 0.63	2 ± 0	1.83 ± 0.41	2 ± 0	2 ± 0
Padding and synchondrosis	1.33 ± 0.52	0.33 ± 0.52	1.67 ± 0.52	0.67 ± 0.52	2 ± 0	2 ± 0
Total score	12.17 ± 1.33	5.50 ± 2.07*	13 ± 1.55	9.33 ± 1.37*	14 ± 0	14 ± 0*

The total score has a range of 0–14: 0 refers to the normal cartilage and 14 refers to completely unrepaired cartilage

*$P < 0.05$

good stability and mechanical support for articular cartilage repair [26]. The lack of obvious physical interface between the bone and cartilage layers in our study was consistent with these effects.

In preliminary studies we found that the use of only sodium alginate and hydroxyapatite as matrix materials could cause collapse during 3D printing, whereas the addition of certain proportion of gelatin allowed the gel scaffold to remain in a designed state prior to crosslinking. Gelatin is a temperature-sensitive natural polymer material with good biocompatibility and biodegradability that dissolves into a liquid state at 25 °C and gels below 10 °C. Therefore, providing 4 °C to 10 °C range of environment temperature for the gelatin in the printed material to solidify rapidly and prevent the material from collapsing, completing the scaffold material curing process smoothly. How about the low temperature influence on seed cells in the printing material? The cells and tissues usually die of cryodamage by the ice crystals formation inside and outside of cells. While, in our experiment, the whole printing process took less than 3 min, and it would not cause the cells to form ice crystals within the experimental temperature range. After the printing, we carried out CAM/PI fluorescence staining to observe cell growth in the scaffold, and found that although there were many dead cells, living cells still accounted for the vast majority. So the printing process including temperature certainly had an effect on cell viability, but the effect was not significant. It wouldn't affect subsequent transplantation experiments.

The cytotoxicity test results of the integrated scaffold materials indicated that the prepared integrated osteochondral scaffold has good biocompatibility, along with degradability and certain mechanical strength, thereby providing a good space for cell growth in the articular cartilage defect. Suitable pore size and porosity likely contribute to the exchange of substances between the scaffold layers, facilitating chondrocyte and bone cell proliferation and extracellular matrix secretion in the defect.

The integrated osteochondral tissues are gelatinous after printing and in vitro culture, with no pressure-bearing ability. After implantation into the animal body, the pressure on the graft is largely borne by the osteochondral tissue surrounding the defect. As time goes on, the scaffold material gradual degrades and the seed cells and autologous tissue grow into the body; the repaired tissue eventually exhibits certain mechanical properties. After 3 and 6 months, the integrated tissue mechanical properties were significantly improved compared with those of the original gelatinous tissue, but differed significantly from normal cartilage tissue, suggesting that a longer repair time or further improvement in repair methods is necessary.

Mature articular cartilage lacks blood supply and nerve distribution, and articular cartilage injury is often accompanied by subchondral bone damage. Moreover, mechanical support of the subchondral bone plays a key role in cartilage repair [27]. As bone-to-bone interface binding is easier to generate, stronger, and more effective than bone-to-cartilage or cartilage-to-cartilage interface binding [28], binding to the subchondral bone may provide the physiological and mechanical environment for cartilage regeneration as required. This suggests that osteochondral repair should be achieved as a whole, concurrent with the repair of hyaline cartilage and subchondral bone.

Our findings in the untreated group confirmed that cartilage defects larger than 3 mm cannot undergo natural repair [29], whereas the implanted scaffold alone could provide a stable environment for osteochondral repair, suggesting that endogenous stem cells may be involved in the repair of cartilage; however, the cell number is limited. In the experimental group, at 6 months after implantation, the repaired tissues in the experimental group were firmly bonded to the surrounding tissue and a tide mark, the iconic structure of mature cartilage, appeared [30]. These findings suggest that the new cartilage tissue had a certain functional structure, which basically achieved the repair effect despite the appearance of a "transition zone" earlier in the process wherein the binding sites appeared easy to separate under external force. Induced BMSCs combined with the integrated osteochondral scaffold could provide more stem cells, and integration of the cartilage layer and the subchondral bone layer facilitated the repair of articular cartilage and subchondral bone. Moreover, the repaired cartilage and subchondral bone were better than those repaired by the simple scaffold without cells.

The 3D printed integrated osteochondral scaffold not only simulates the normal osteochondral structure, but also biosimulates the natural osteochondral component, achieving the dual bionics of structure and composition, finally implementing effective bone repair and regeneration. However, the normal osteochondral tissue has complex anatomical structure and composition. There are also dynamic changes in the time and space of the regeneration zone during the repair and regeneration process. Rather than the simple filling of new tissues, it is necessary to regenerate the subchondral bone supporting the hyaline cartilage, along with the hyaline articular cartilage that is tightly bound to the bone, thereby realizing formation of the cartilage and bone interface and concurrent regeneration of the cartilage and bone. Regardless, a specific material similar to the natural osteochondral tissue has not yet been realized. In addition, the calcified layer and the tide mark play important roles in the osteochondral structure [31–33], which are unable to be completely simulated by the integrated bionic scaffold [34, 35]. Moreover, calcification of the cartilage layer and easy delamination of biphasic or polyphase scaffolds [36] remain concerns. 3D bioprinted integrated osteochondral

tissue scaffolds, which achieve a dual bionics of the normal cartilage in terms of structure and composition, are thus expected to become a new strategy for osteochondral repair and regeneration.

Overall, the 3D bioprinted integrated osteochondral scaffold could promote the repair of osteochondral defects in the weight-bearing area of the rabbit joint. After 6 months of implantation, the quality of the repaired cartilage was similar to that of the surrounding normal cartilage. However, further investigations on the long-term effect are necessary.

Acknowledgements This research was supported by the Natural Science Foundation of Zhejiang Province of China (Nos. LY18H180010, LY17H060011, and LY17H280008), grants from the Zhejiang Provincial Medical Science and Technology Plan Project of China (Nos. 2015KYB092, 2017KY307, 2017KY299, 2017KY303, and 2019KY364), and grants from Zhejiang Provincial Traditional Chinese Medicine Science and Technology Plan Project of China (Nos. 2016ZA044, 2015ZA045, and 2018ZA017).

References

1. Baghaban, E. M., & Malakooty, P. E. (2014). Mesenchymal stem cells as a potent cell source for articular cartilage regeneration. *World Journal of Stem Cells, 6,* 344–354.
2. Gratz, K. R., Wong, V. W., Chen, A. C., Fortier, L. A., Nixon, A. J., & Sah, R. L. (2006). Biomechanical assessment of tissue retrieved after in vivo cartilage defect repair: Tensile modulus of repair tissue and integration with host cartilage. *Journal of Biomechanics, 39,* 138–146.
3. Jiang, J., Tang, A., Ateshian, G. A., Guo, X. E., Hung, C. T., & Lu, H. H. (2010). Bioactive stratified polymer ceramic-hydrogel scaffold for integrative osteochondral repair. *Annals of Biomedical Engineering, 38,* 2183–2196.
4. Biao-Qi, C., Ranjith, K., Ai-Zheng, C., Ding-Zhu, Y., Xiao-Xia, C., Ni-Na, J., et al. (2017). Investigation of silk fibroin nanoparticle-decorated poly(l-lactic acid) composite, scaffolds for osteoblast growth and differentiation. *International Journal of Nanomedicine, 12,* 1877–1890.
5. Yang, Q., Peng, J., Guo, Q., Huang, J., Zhang, L., Yao, J., et al. (2008). A cartilage EMC-derived 3-D porous acellular matrix scaffold for in vivo cartilage tissue engineering with PKH26-labeled chondrogenic bone marrow-derived mesenchymal stem cells. *Biomaterials, 29,* 2378–2387.
6. Melissa, L. M., Greet, M., Jessica, R., Pascal, G., Petra, H., Peter, C., et al. (2018). Stem cells for cartilage repair: Preclinical studies and insights in translational animal models and outcome measures. *Stem Cells International, 2018,* 9079538.
7. Harley, B. A., Lynn, A. K., Wissner-Gross, Z., Bonfield, W., Yannas, I. V., & Gibson, L. J. (2010). Design of a multiphase osteochondral scaffold iii: Fabrication of layered scaffolds with continuous interfaces. *Journal of Biomedical Materials Research, Part A, 92A,* 1078–1093.
8. Kankala, R. K., Zhu, K., Li, J., Wang, C. S., Wang, S. B., & Chen, A. Z. (2017). Fabrication of arbitrary 3d components in cardiac surgery: From macro-, micro- to nanoscale. *Biofabrication, 9,* 032002.
9. Neary, M., Barron, V., Barry, F., Shannon, F., & Murphy, M. (2018). Cartilage repair in a rabbit model: Development of a novel subchondral defect and assessment of early cartilage repair using rabbit mesenchymal stem cell seeded scaffold. *Irish Journal of Medical Science, 183,* S249–S250.
10. Park, J. Y., Choi, J. C., Shim, J. H., Lee, J. S., & Cho, D. W. (2014). A comparative study on collagen type I and hyaluronic acid dependent cell behavior for osteochondral tissue bioprinting. *Biofabrication, 6,* 035004.
11. O'Reilly, A., & Kelly, D. J. (2016). A computational model of osteochondral defect repair following implantation of stem cell-laden multiphase scaffolds. *Tissue Engineering Part A, 23,* 30–42.
12. Georgi, N., Van Blitterswijk, C., & Karperien, M. (2014). Mesenchymal stromal/stem cell- or chondrocyte-seeded microcarriers as building blocks for cartilage tissue engineering. *Tissue Engineering Part A, 20,* 2513–2523.
13. Tritzschiavi, J., Charif, N., Henrionnet, C., De, I. N., Bensoussan, D., Magdalou, J., et al. (2010). Original approach for cartilage tissue engineering with mesenchymal stem cells. *BioMedical Materials and Engineering, 20,* 167–174.
14. Lam, J., Lu, S., Lee, E. J., Trachtenberg, J. E., Meretoja, V. V., Dahlin, R. L., et al. (2014). Osteochondral defect repair using bilayered hydrogels encapsulating both chondrogenically and osteogenically pre-differentiated mesenchymal stem cells in a rabbit model. *Osteoarthritis and Cartilage, 22,* 1291–1300.
15. Meng, Y. H., Zhu, X. H., Yan, L. Y., Zhang, Y., Jin, H. Y., Xia, X., et al. (2016). Bone mesenchymal stem cells improve pregnancy outcome by inducing maternal tolerance to the allogeneic fetus in abortion-prone matings in mouse. *Placenta, 47,* 29–36.
16. Ma, G., Zhao, J. L., Mao, M., Chen, J., & Liu, Y. P. (2016). Scaffold-based delivery of bone marrow mesenchymal stem cell sheet fragments enhances new bone formation in vivo. *Journal of Oral and Maxillofacial Surgery: Official Journal of the American Association of Oral and Maxillofacial Surgeons, 75,* 92–104.
17. Yin, H., Wang, Y., Sun, Z., Sun, X., Xu, Y., Li, P., et al. (2016). Induction of mesenchymal stem cell chondrogenic differentiation and functional cartilage microtissue formation for in vivo cartilage regeneration by cartilage extracellular matrix-derived particles. *Acta Biomaterialia, 33,* 96–109.
18. Zhang, W. Y., Yang, Y. D., He, C., & Chen, Y. (2004). Isolation culture and esteogenic differentiation of rabbit bone marrow-derived mesenchymal stem cells. *Zhejiang Practical Medicine, 9,* 393–395.
19. Zhang, W. Y., Yang, Y. D., He, C., & Chen, Y. (2004). Experimental studies of osteogenic and chondrogenic potentiality of rabbit bone marrow-derived mesenchymal stem cells. *Modern Medicine Health, 20,* 2083–2085.
20. Yadong, Y., Wenyuan, Z., Ying, L., Guojian, F., & Keji, Z. (2014). Scalded skin of rat treated by using fibrin glue combined with allogeneic bone marrow mesenchymal stem cells. *Annals of Dermatology, 26,* 289–295.
21. Lee, W., Debasitis, J. C., Lee, V. K., Lee, J. H., Fischer, K., Edminster, K., et al. (2009). Multi-layered culture of human skin fibroblasts and keratinocytes through three-dimensional freeform fabrication. *Biomaterials, 30,* 1587–1595.
22. Wakitani, S., Goto, T., Pineda, S. J., Young, R. G., Mansour, J. M., Caplan, A. I., et al. (1994). Mesenchymal cell-based repair of large, full-thickness defects of articular cartilage. *Journal of Bone and Joint Surgery-American, 76,* 579–592.
23. Fragonas, E., Valente, M., Pozzimucelli, M., Toffanin, R., Rizzo, R., Silvestri, F., et al. (2000). Articular cartilage repair in rabbits by using suspensions of allogenic chondrocytes in alginate. *Biomaterials, 21,* 795–801.
24. Filion, T. M., Li, X., Mason-Savas, A., Kreider, J. M., Goldstein, S. A., Ayers, D. C., et al. (2011). Elastomeric osteoconductive synthetic scaffolds with acquired osteoinductivity expedite the repair of critical femoral defects in rats. *Tissue Engineering Part A, 17,* 503–511.

25. Jiang, J., Hao, W., Li, Y., Yao, J., Shao, Z., Li, H., et al. (2013). Hydroxyapatite/regenerated silk fibroin scaffold-enhanced osteoinductivity and osteoconductivity of bone marrow-derived mesenchymal stromal cells. *Biotechnology Letters, 35,* 657–661.
26. Xue, D., Zheng, Q., Zong, C., Li, Q., Li, H., Qian, S., et al. (2010). Osteochondral repair using porous poly(lactide-co-glycolide)/nano-hydroxyapatite hybrid scaffolds with undifferentiated mesenchymal stem cells in a rat model. *Journal of Biomedical Materials Research, Part A, 94A,* 259–270.
27. Araki, S., Imai, S., Ishigaki, H., Mimura, T., Nishizawa, K., Ueba, H., et al. (2015). Improved quality of cartilage repair by bone marrow mesenchymal stem cells for treatment of an osteochondral defect in a cynomolgus macaque model. *Acta Orthopaedica, 86,* 119–126.
28. Kalson, N. S., Gikas, P. D., & Briggs, T. W. (2010). Current strategies for knee cartilage repair. *International Journal of Clinical Practice, 64,* 1444–1452.
29. Freed, L. E., Grande, D. A., Lingbin, Z., Emmanual, J., Marquis, J. C., & Langer, R. (2010). Joint resurfacing using allograft chondrocytes and synthetic biodegradable polymer scaffolds. *Journal of Biomedical Materials Research, Part A, 28,* 891–899.
30. Zhang, W., Lian, Q., Li, D., Wang, K., Jin, Z., Bian, W., et al. (2014). cartilage repair and subchondral bone reconstruction based on three-dimensional printing technique. *Chinese Journal of Reparative and Reconstructive Surgery, 28,* 318–324.
31. Wang, F., Yang, L., Duan, X., Tan, H., & Dai, G. (2008). Study on shape and structure of calcified cartilage zone in normal human knee joint. *Chinese Journal of Reparative and Reconstructive Surgery, 27,* 524–527.
32. Havelka, S., Horn, V., Spohrová, D., & Valouch, P. (1984). The calcified–noncalcified cartilage interface: The tidemark. *Acta Biologica Hungarica, 35,* 271–279.
33. Mansfield, J. C., & Winlove, C. P. (2012). A multi-modal multiphoton investigation of microstructure in the deep zone and calcified cartilage. *Journal of Anatomy, 220,* 405–416.
34. Dua, R., Centeno, J., & Ramaswamy, S. (2014). Augmentation of engineered cartilage to bone integration using hydroxyapatite. *Journal of Biomedical Materials Research. Part B, Applied Biomaterials, 102,* 922–932.
35. Nosewicz, T. L., Reilingh, M. L., Wolny, M., Dijk, C. N. V., & Schell, H. (2013). Influence of basal support and early loading on bone cartilage healing in press-fitted osteochondral autografts. *Knee Surgery, Sports Traumatology, Arthroscopy, 22,* 1445–1451.
36. Viti, F., Scaglione, S., Orro, A., & Milanesi, L. (2014). Guidelines for managing data and processes in bone and cartilage tissue engineering. *BMC Bioinformatics, 15,* S14.